35th Annual International Conference of the IEEE EMBS
Osaka, Japan, 3 - 7 July, 2013

FEM electrode refinement for Electrical Impedance Tomography

Bartłomiej Grychtol[1] and Andy Adler[2]

Abstract— **Electrical Impedance Tomography (EIT) reconstructs images of electrical tissue properties within a body from electrical transfer impedance measurements at surface electrodes. Reconstruction of EIT images requires the solution of an inverse problem in soft field tomography, where a sensitivity matrix, J, of the relationship between internal changes and measurements is calculated, and then a pseudo-inverse of J is used to update the image estimate. It is therefore clear that a precise calculation of J is required for solution accuracy. Since it is generally not possible to use analytic solutions, the finite element method (FEM) is typically used. It has generally been recommended in the EIT literature that FEMs be refined near electrodes, since the electric field and sensitivity is largest there. In this paper we analyze the accuracy requirement for FEM refinement near electrodes in EIT and describe a technique to refine arbitrary FEMs.**

I. INTRODUCTION

Electrical Impedance Tomography (EIT) reconstructs images of electrical tissue properties within a body from electrical transfer impedance measurements at surface electrodes. For biomedical imaging applications, it is being actively studied for monitoring the movement of air and blood in the thorax, and for imaging the head and breast. Reconstruction of EIT images requires the solution of an inverse problem in soft field tomography. EIT imaging requires an iterative solution in which, at each step, a sensitivity matrix, $\mathbf{J}$, of the relationship between internal changes and measurements is calculated, and then a pseudo-inverse of $\mathbf{J}$ is used to update the image estimate. (Several algorithms use one step of the iterative solution.) EIT image reconstruction is ill-posed, since the physics of current propagation imply that sensitivity is largest near the electrodes and smallest in the body center.

It is therefore clear that a precise calculation of $\mathbf{J}$ is required for solution accuracy. Since it is generally not possible to use analytic solutions (because of the non-regular shapes of biological bodies and the boundary conditions on a conductive electrode) the finite element method (FEM) is typically used. One key advantage of FEM is that element size can be selectively refined in regions to meet solution accuracy. Thus it has generally been recommended in the EIT literature that FEMs be refined near electrodes, since the electric field and sensitivity is largest there. However, we have identified two problems with this recommendation. First, no careful analysis has been made to determine how much refinement is required. Given an "FEM element budget", how much should be "spent" on elements near electrodes vs. in the body core? Next, there is a lack of freely available mesh generation tools to refine FEM electrodes on arbitrary body shapes. Most commercially available FEM packages do not conveniently provide such capability either.

In this paper our goals are: 1) to analyze the accuracy requirement for FEM refinement near electrodes in EIT, and 2) to make freely available a technique to refine arbitrary FEMs.

II. METHODS

A. Overview

A cylinder ($\varnothing = 0.5$ m, height $h = 0.25$ m) with four square electrodes (5 cm edge length) placed equidistantly around the perimeter at mid-height was meshed with Netgen [1]. Several meshes with different number of tetrahedra with and without electrode refinement were generated. Assuming a uniform conductivity of 1 Sm^{-1}, we used each mesh to calculate the potential distribution caused by a current of 1 A passing between two adjacent electrodes, and simulated a measurement of potential difference between the other two electrodes. We also calculated the sensitivity of the measurement to conductivity changes in the electrode plane. Results were compared against those obtained using the finest mesh. All calculations were performed in Matlab (The Mathworks, Natick, MA, USA) using EIDORS [2].

B. Mesh Generation

Meshes of different size were generated with Netgen by manipulating the desired maximum edge length (maxh parameter) for the entire domain and the electrodes, leaving all other meshing options at their default values. The values were chosen such as to divide the electrode side of 5 cm into an integer number of segments of equal size. Example meshes are presented in Fig. 1.

Two types of mesh were generated. In models C0–C7, the desired mesh size in the entire medium and the electrodes were equal, the number indicating the level of coarsening with respect to the finest model C0. In models R1–R7, local refinement around the electrodes was achieved by decreasing the desired mesh size of the electrode while keeping that for the entire domain constant and equal to that in the coarsest mesh C7. The settings used to generate all fifteen meshes and their sizes are reported in Table I together with the time taken to calculate the potential distribution as described next on a powerful server.

[1]B. Grychtol is with the Department of Medical Physics in Radiology, German Cancer Research Center, 69120 Heidelberg, Germany b.grychtol at dkfz.de

[2]A. Adler is with Systems and Computer Engineering, Carleton University, Ottawa, ON, Canada K1S 5B6 adler at sce.carleton.ca

The work of B. Grychtol was supported by a fellowship from the Alexander von Humboldt Foundation.

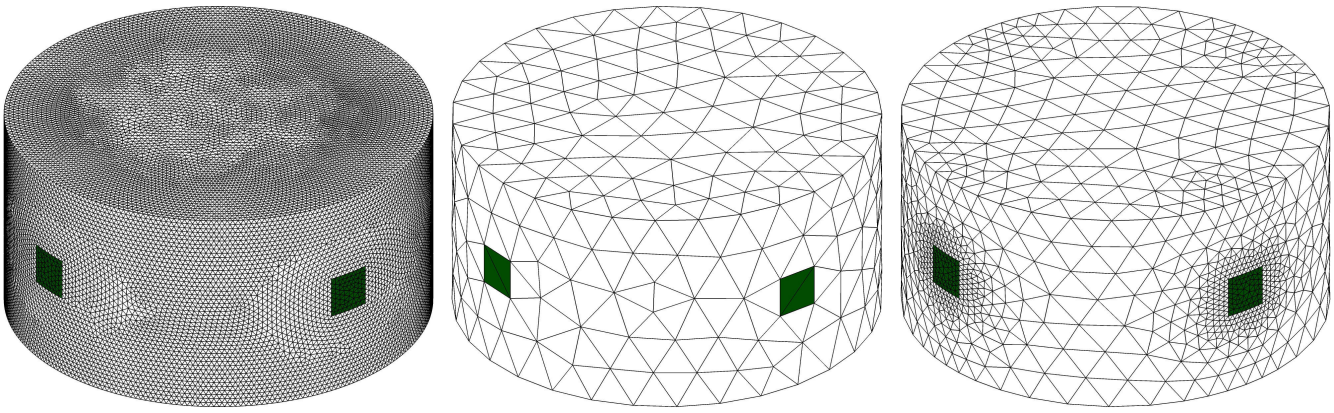

(a) C0 (b) C7 (c) R7

Fig. 1: Examples of (a) fine, (b) coarse and (c) refined meshes.

TABLE I: Mesh characteristics and measurement simulation time

Model	C0	C1	C2	C3	C4	C5	C6	C7	R1	R2	R3	R4	R5	R6	R7
global maxh [mm]	6.25	7.14	8.33	10	12.5	16.7	25	50	50	50	50	50	50	50	50
elec. maxh [mm]	6.25	7.14	8.33	10	12.5	16.7	25	50	25	16.7	12.5	10	8.33	7.14	6.25
# elem. per elec. edge	8	7	6	5	4	3	2	1	2	3	4	5	6	7	8
# elements	1291473	1254681	633324	230947	160323	79787	19033	1983	3705	7893	14538	17778	23423	31188	38244
# nodes	233640	224963	114363	43941	30642	15290	4047	524	874	1712	2956	3601	4692	6098	7436
# elec. elem.	138	110	74	56	36	22	6	2	6	22	28	50	72	86	104
minEL[a] [mm]	3.37	3.55	3.95	5.53	6.7	9.1	13.9	35.4	17.9	11.9	8.2	6.76	5.34	4.94	4.25
maxEL[b] [mm]	15.4	15	19.1	25.2	30.9	41.4	52.3	103	96.1	84.2	85.5	82.7	75.3	73.5	74.4
minEV[c] [cm^3]	0.00825	0.00888	0.0146	0.0407	0.0565	0.139	0.514	8.03	1.55	0.303	0.123	0.0814	0.034	0.0234	0.0131
maxEV[d] [cm^3]	0.159	0.159	0.405	0.739	1.14	3.62	8.67	71.2	59.7	46.1	28.3	31	25.4	26.5	25.2
simulation time[e] [s]	86	82.6	34.4	10.7	7.19	3.37	0.796	0.103	0.171	0.337	0.601	0.749	0.98	1.3	1.61

[a] length of the shortest edge; [b] length of the longest edge; [c] volume of the smallest element; [d] volume of the largest element; [e] average of ten runs.

C. Simulation

The potential at each node $\mathbf{V}$ of the mesh was calculated using the finite element method (FEM) using the linearization

$$\mathbf{V} = \mathbf{Y}^{-1}\mathbf{C} \tag{1}$$

where $\mathbf{Y}$ is the admittance matrix of the FEM (and a function of conductivity distribution) and $\mathbf{C}$ is a matrix representing the current injection pattern, such that $\mathbf{C}_{ij}$ represents the current injected in electrode i during the j-th stimulation. Here, we drive current of 1 A between two adjacent electrodes in a single stimulation, so $C = [0\,|\,0\,|\,1\,|\,-1]^T$. We pick a node in the center of the FEM as ground, since it is necessary to assume the potential on one node for $\mathbf{Y}$ to be invertible [3]. We use the complete electrode model and assume contact impedance of 0.01 Ω in the calculation of the admittance matrix [4]. The resultant potential distribution in the electrode plane, calculated for the finest mesh and subsequently projected onto a 512×512 pixel grid, is presented in Fig. 2a. The potential distribution $\mathbf{V}$ is used to visualize the current flow around the measuring electrodes.

We calculate the sensitivity (or Jacobian) matrix $\mathbf{J}$ of measurements $\mathbf{v}$ to changes in the conductivity σ of individual elements as $\mathbf{J}_{ij} = \frac{\partial v_j}{\partial \sigma_i}$ using the adjoint method [4]. Again, since we only have one measurement, $\mathbf{J}$ is in fact a vector. We construct a sensitivity image by assigning each element i of the FEM the value of $\mathbf{J}_i$ divided by the element's volume. Mean sensitivity in the plane of electrodes is then calculated by averaging the sensitivity in fifteen planes parallel to the plane of electrodes and spanning the height of 6.67 cm. Results for the finest model are presented in Fig. 2b.

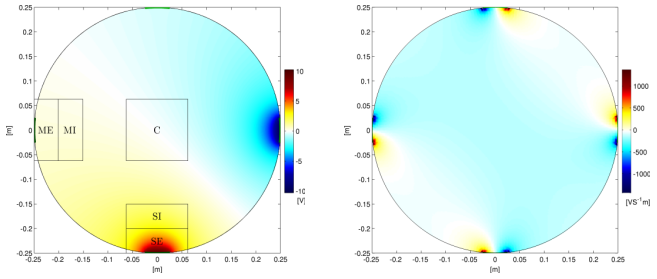

(a) Potential distribution (b) Sensitivity distribution

Fig. 2: Reference results obtained on model C0.

D. Meshing errors

We compare the meshes in terms of the value of the voltage measurement between the non-stimulating electrodes, the distribution of current around the measuring electrodes and the average sensitivity in select regions of interest (ROI) in the electrode plane. The ROIs are indicated in Fig. 2a. We

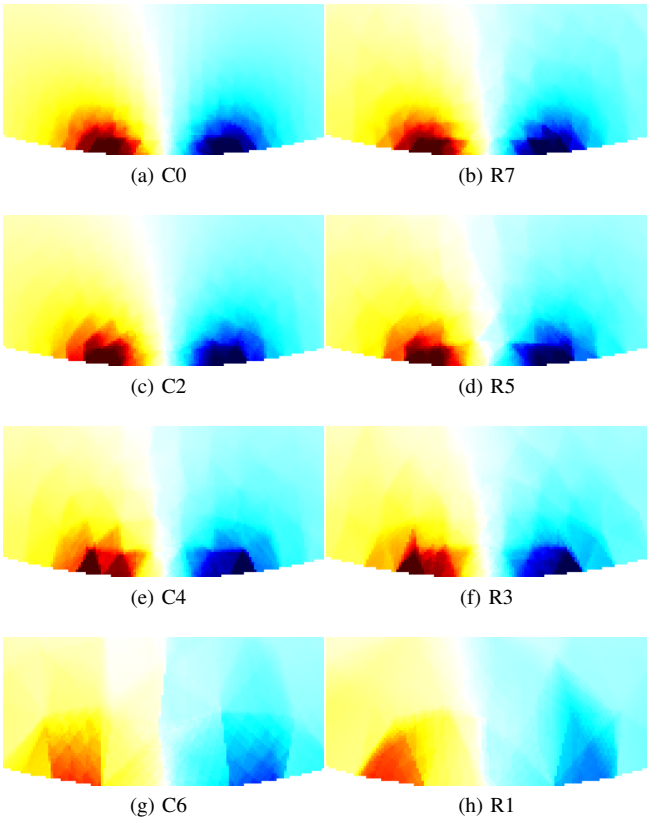

(a) C0 (b) R7

(c) C2 (d) R5

(e) C4 (f) R3

(g) C6 (h) R1

Fig. 3: Average sensitivity in the electrode plane in the vicinity of an electrode (ROIs SE and SI). All images use the same color scale.

use the results obtained with the C0 mesh as reference to compare the others against.

E. Electrode refinement for arbitrary FEMs

Our approach to building arbitrary FEMs with electrode refinement proceeds as follows. Starting with a closed triangular surface mesh and a list of desired electrode shapes and positions, we project the electrode shapes onto the surface adding new nodes along the electrodes' edges and integrating them into the mesh by 2D constrained Delaunay re-triangulation in the neighborhood of the electrode. Subsequently, we extrude the electrode surface slightly outwards and save the surface mesh as an STL file. We then use Netgen to generate a highly optimized tetrahedral mesh, from which we extract the new surface triangulation. The sharp edges around the extruded electrodes force Netgen to preserve their boundaries and produce local refinement. We re-integrate the electrodes into the surface by reversing the extrusion. The resulting surface mesh is finally processed with Gmsh [5], which converts it to a volume mesh without changing the surface, thus propagating the refinement into the volume.

III. RESULTS

Sensitivity is found to be very high in the immediate vicinity of the edges of the electrode and rapidly decreasing

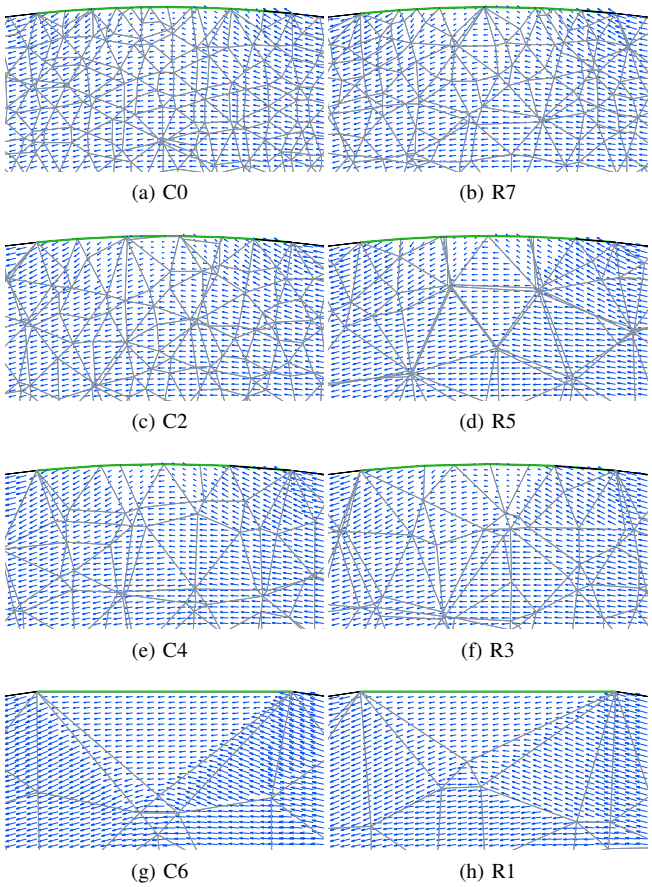

(a) C0 (b) R7

(c) C2 (d) R5

(e) C4 (f) R3

(g) C6 (h) R1

Fig. 4: Current flow in the electrode plane (ROIs ME and MI). Arrows in each image are scaled individually.

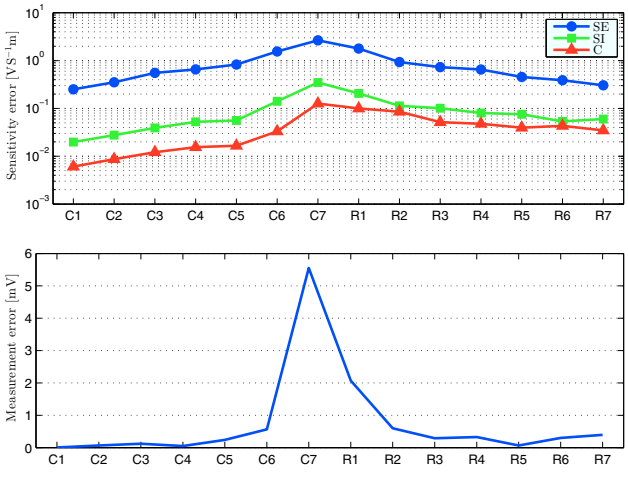

Fig. 5: Errors with respect to model C0.

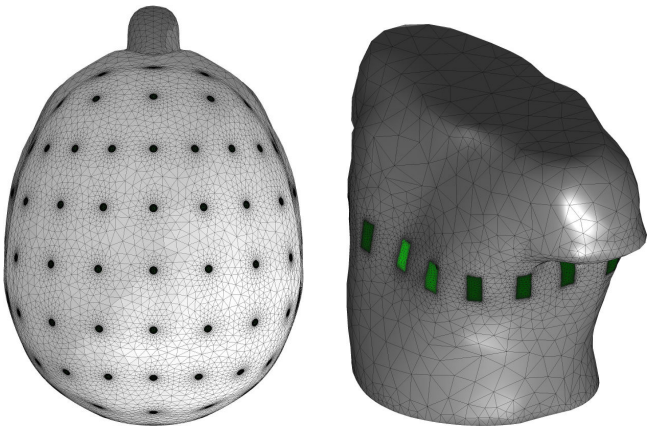

Fig. 6: Example FEMs of a human head (top view, left) and a male thorax (right) with electrode refinement.

away from them (Figures 2b and 3a). This effect is readily explained by the current distribution near the measurement electrode presented in Fig. 4a. The high conductivity of the electrode attracts current near its edges increasing the current density there, and decreasing it under the electrode. This effect, shown in Figures 3 and 4, is increasingly difficult to capture as the size of the elements near the electrode increases, and disappears entirely in the coarsest model (not shown). In both figures, there is little appreciable difference between the homogeneous models (C) and those with electrode refinement (R) with the same number of elements per electrode edge. Thus, the size of elements deep in the medium does not affect the sensitivity near the electrode. This is corroborated by the graph in Fig. 5 showing similar sensitivity errors for the corresponding C and R models in the immediate vicinity of an electrode (ROI SE). Deeper in the medium (ROIs SI and C), the sensitivity error is decreased by electrode refinement but remains higher with respect to the finer homogeneous models, even when those are coarser around the electrode. Compare e.g. models R5 and C6, which have similar number of nodes and elements. Overall, sensitivity varies substantially between the models, especially near the electrode.

In contrast, the measurement error, with a maximum value of 5.5 mV on the coarsest model C7 and below 1 mV for all other models (Fig. 5), is relatively small considering that the measurement obtained on model C0 was 885 mV.

IV. DISCUSSION

We consider the requirement of FEM refinement in the neighborhood of electrodes in EIT. While such refinement is generally agreed to be useful, we have identified two problems: a lack of systematic analysis of the required refinement level, and a difficulty in implementing such refinement on arbitrary FE models. We presents contributions in both areas.

First, the benefit of electrode refinement has been analysed by considering a sequence of refined FEMs compared to a "gold standard", uniformly fine FEM solution. The models were refined either globally or in the electrode neighborhood, and the voltage measurement, current distribution and sensitivity were compared. Results are summarized in Fig. 5 which indicates that model errors near the electrodes decrease equally with electrode and uniform refinement. Model errors deeper in the body are improved with electrode refinement, but not as much as by uniform refinement (as would be expected). However, since errors deeper in the body are so much smaller, this may be less of a factor in many scenarios.

Second, we have developed a procedure to place circular or rectangular electrodes on an arbitrary closed triangular surface mesh based exclusively on open source software. To the best of the authors' knowledge, no free pre-compiled tool exists to build meshes of arbitrary geometries, as extracted e.g. from computed tomography (CT) data, with electrode refinement. Commercial FE modeling tools also do not offer an easy interface to perform electrode refinement. While our method combining two programs over whose results we do not have full control is not without caveats, it addresses this important need in the modeling community. The procedure has been contributed to the EIDORS project and will be part of the next release (3.7). We present two example meshes based on models previously contributed to EIDORS but lacking electrode refinement [6], [7] in Fig. 6.

In summary, as expected, refinement of electrode meshes near electrodes does improve model accuracy in terms of calculated voltage and sensitivity, while offering much shorter calculation times than uniformly fine models. We recommend that, for each EIT imaging case, required model accuracy be determined from an analysis of the system, and then the required electrode refinement be determined from Fig. 5. Additionally, we recommend that a minimum of four FEM elements be used on any electrode model, to capture the dynamics of current flow. Further to these recommendations, by contributing freely available tools and tutorials for such electrode refinement, we hope to facilitate such improved FE modeling in EIT.

REFERENCES

[1] J. Schöberl, "NETGEN An advancing front 2D/3D-mesh generator based on abstract rules," *Computing and Visualization in Science*, vol. 1, no. 1, pp. 41–52, July 1997.

[2] A. Adler and W. R. B. Lionheart, "Uses and abuses of EIDORS: an extensible software base for EIT." *Physiological measurement*, vol. 27, no. 5, pp. S25–42, May 2006.

[3] A. Adler and R. Guardo, "Electrical impedance tomography: regularized imaging and contrast detection." *IEEE Trans. Med. Imag.*, vol. 15, no. 2, pp. 170–9, Jan. 1996.

[4] N. Polydorides and W. R. B. Lionheart, "A Matlab toolkit for three-dimensional electrical impedance tomography: a contribution to the Electrical Impedance and Diffuse Optical Reconstruction Software project," *Measurement Science and Technology*, vol. 13, no. 12, pp. 1871–1883, Dec. 2002.

[5] C. Geuzaine and J.-F. Remacle, "Gmsh: A 3-D finite element mesh generator with built-in pre- and post-processing facilities," *International Journal for Numerical Methods in Engineering*, vol. 79, no. 11, pp. 1309–1331, Sept. 2009.

[6] A. Tizzard and R. H. Bayford, "Improving the finite element forward model of the human head by warping using elastic deformation." *Physiological measurement*, vol. 28, no. 7, pp. S163–82, July 2007.

[7] A. Adler et al., "GREIT: a unified approach to 2D linear EIT reconstruction of lung images." *Physiological measurement*, vol. 30, no. 6, pp. S35–55, June 2009.